

FR 7601697

A STUDY OF THE $^{12}\text{C}(\alpha, ^8\text{Be})^8\text{Be}$ REACTION IN THE ENERGY
RANGE $E_\alpha = 17 - 33$ MeV

F. Brochard, P. Chevallier, D. Didier, V. Rauch,
G. Rudolf et F. Scheibling

Centre de Recherches Nucléaires and Université Louis
Pasteur, Strasbourg, France

Institut National
de Physique Nucléaire
et de Physique
des Particules

Université
Louis Pasteur
de Strasbourg

1. THE REACTION $^{12}\text{C}(^{8}\text{Be}, ^{16}\text{O})$ AT HIGH ENERGIES AND ANGLES

F. BECHTOLD, *Physikalisches Institut der Universität Bonn*

FRANZ KLEIN

Physikalisches Institut der Universität Bonn, Institut für Experimentelle

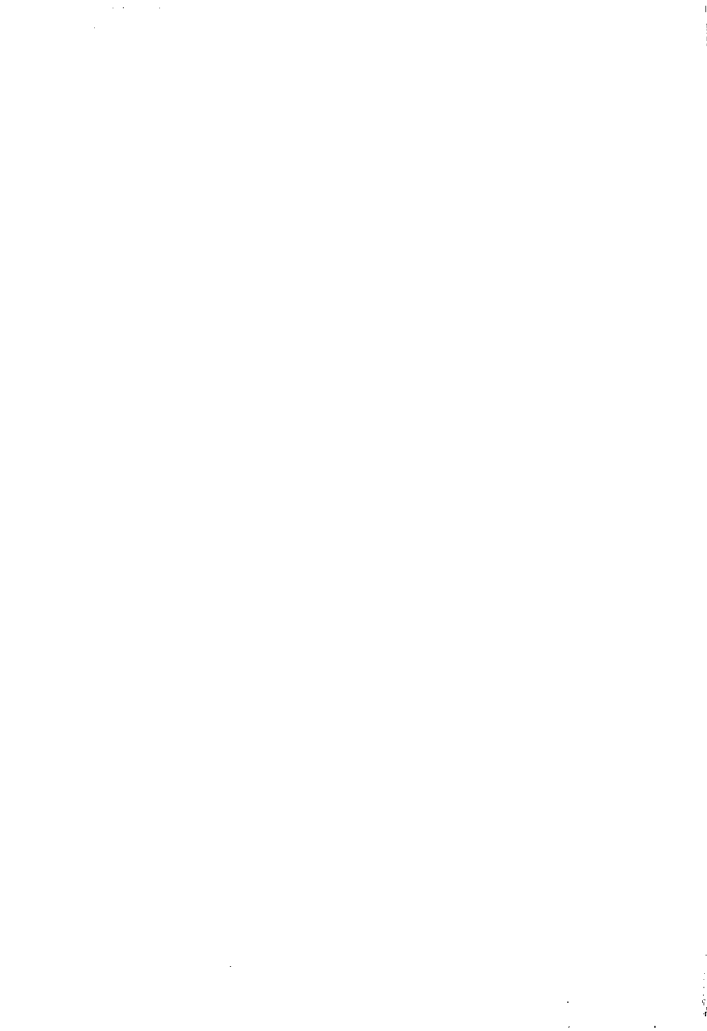
Strukturphysik Bonn

The reaction functions and angular distributions for the $^{12}\text{C}(^{8}\text{Be}, ^{16}\text{O})$ reaction were measured for $E_{\text{lab}} = 7 - 33$ MeV. Numerous resonances were observed, except for a narrow resonance at $E_{\text{lab}} = 12.56$ MeV. Total and inelastic cross sections are determined from the angular distributions. Below $E_{\text{lab}} = 10$ MeV no $l = 2$ contribution was found. For higher energies an $l = 2$ contribution appears, increases gradually and becomes dominant at and above $E_{\text{lab}} = 13$ MeV. A tentative interpretation of the behavior of $^{12}\text{C}(^{8}\text{Be}, ^{16}\text{O})$ partial cross sections is given in the framework of the Hauser-Feshbach formalism.

[NUCLEAR REACTIONS $^{12}\text{C}(^{8}\text{Be}, ^{16}\text{O})$, $E = 7 - 33$ MeV, measured $\sigma(E, \theta)$, ^{16}O resonances, natural targets.]

1. INTRODUCTION

The large number of resonances identified in the work of Chevallier et al.¹ shows that the $^{12}\text{C}(^{8}\text{Be}, ^{16}\text{O})$ reaction seems to be particularly well adapted to study the high energy structure of the ^{16}O nucleus. These results were confirmed by Martin and Ophel² who studied the same reaction in the incident energy range $E_{\text{lab}} = 15 -$



1. CHEVILLIER, J., *Be⁸ et ¹²C*, Centre National de la Recherche Scientifique, Paris, 1967.

2. B. B. BLOOM, *J. Nuclear Energy, C*, **10**, 109 (1966).

3. B. B. BLOOM, *ibid.*, **11**, 109 (1967).

4. G. B. BLOOM, *ibid.*, **12**, 109 (1968).

5. G. B. BLOOM, *ibid.*, **13**, 109 (1969).

Excitation functions and angular distributions for the $^{12}\text{C}(\alpha, \text{Be})^8\text{Be}$ reaction were measured for $E_\alpha = 7 - 13$ MeV. Angular distributions were observed, except for a narrow resonance at $E_\alpha = 12.0$ MeV. Total and partial cross sections are determined from the angular distributions. Below $E_\alpha = 10$ MeV no $l = 8$ resonance was detected. For higher energies an $l = 8$ contribution appears, increases gradually, and becomes dominant at and above $E_\alpha = 13$ MeV. A tentative interpretation of the behavior of $^{12}\text{C}(\alpha, \text{Be})^8\text{Be}$ partial cross sections is given in the framework of the Hauser-Feshbach formalism.

[NUCLEAR REACTIONS $^{12}\text{C}(\alpha, \text{Be})^8\text{Be}$, $E_\alpha = 7 - 13$ MeV, measured
for $E_\alpha = 7 - 13$ MeV, ^{16}O resonances, natural targets.]

1. INTRODUCTION

The large number of resonances identified in the work of Chevallier *et al.*¹ shows that the $^{12}\text{C}(\alpha, \text{Be})^8\text{Be}$ reaction seems to be particularly well adapted to study the high energy structure of the ^{16}O nucleus. These results were confirmed by Martin and Ophel² who studied the same reaction in the incident energy range $E_\alpha = 15 -$

19 MeV. They showed that in their upper energy region the highest contributing relative angular momentum for $^{12}\text{C} + \alpha$ is $L = 8$. The corresponding partial cross section was found to be dominant up to $E_{\alpha} = 22$ MeV simultaneously by James et al.³⁾ and Brochard et al.⁴⁾

The present investigation of the $^{12}\text{C}(\alpha, ^8\text{Be})^8\text{Be}$ reaction was undertaken with the principal intent of studying high spin levels in ^{12}C and especially to search for the $J^{\pi} = 8^{+}$ level belonging to a suggested 8 particle - 8 hole band in this nucleus⁵. We have measured excitation functions and angular distributions in the incident energy range $E_{\alpha} = 17 - 33$ MeV. Analysis of the results shows no evidence for a $J^{\pi} = 8^{+}$ state below $E_{\alpha} = 20$ MeV. Above this energy broad structures corresponding to $L = 8$ are found. The structures observed in the L-partial cross sections are compared to the predictions of a statistical Hauser-Feshbach model calculation done with a $^8\text{Be} + ^8\text{Be}$ optical potential of the type used in the description of several low energy heavy-ion reactions.

II. EXPERIMENTAL METHOD

The experiment was performed with the α^{++} beam delivered by the Strasbourg M.P. Tandem accelerator. The beam entered an Ortec scattering chamber through a series of 1 and 2 mm diam collimators. The targets consisted of 20 - 50 $\mu\text{g}/\text{cm}^2$ thick, self-supporting natural carbon foils. Typical beam intensity and integrated charge were respectively 10 - 50 nA and 10 μC per data point.

19 MeV. They showed that in their upper energy region the highest contributing relative angular momentum for $^{12}\text{C} + \alpha$ is $L = 6$. The corresponding partial cross section was found to be dominant up to $E_{\alpha} = 22$ MeV simultaneously by James et al.³ and Brochard et al.⁴

The present investigation of the $^{12}\text{C}(\alpha, ^8\text{Be})^8\text{Be}$ reaction was undertaken with the principal intent of studying high spin levels in ^{12}C and especially to search for the $J^{\pi} = 8^{+}$ level belonging to a suggested 8 particle - 8 hole band in this nucleus⁵. We have measured excitation functions and angular distributions in the incident energy range $E_{\alpha} = 17 - 33$ MeV. Analysis of the results shows no evidence for a $J^{\pi} = 8^{+}$ state below $E_{\alpha} = 20$ MeV. Above this energy broad structures corresponding to $L = 8$ are found. The structures observed in the L-partial cross sections are compared to the predictions of a statistical Hauser-Feshbach model calculation done with a $^8\text{Be} + ^8\text{Be}$ optical potential of the type used in the description of several low energy heavy-ion reactions.

11. EXPERIMENTAL METHOD

The experiment was performed with the α^{++} beam delivered by the Strasbourg M.P. Tandem accelerator. The beam entered an Ortec scattering chamber through a series of 1 and 2 mm diam collimators. The targets consisted of 20 - 50 $\mu\text{g}/\text{cm}^2$ thick, self-supporting natural carbon foils. Typical beam intensity and integrated charge were respectively 10 - 50 nA and 10 μC per data point.

The main experimental task was to find the most favorable geometry for the ^6Be detector system. The detector efficiency was measured by the evaluation of the ^6Be detector signals through a series of measurements for various target-to-detector distances. The ^6Be energy distribution at different angles was obtained from a ^6Be energy distribution at a fixed angle. The angular distribution of ^6Be is made on the basis of theoretical calculations for the reaction $^6\text{Li}(p, \alpha)^6\text{Be}$. The ^6Be particles from the two reactions, $^6\text{Li}(p, \alpha)^6\text{Be}$ and $^6\text{Li}(p, \alpha)^6\text{Be}$, were separated and the detected ^6Be particles were analyzed in the same spectrum of the ^6Li incident energies. Other possible processes give continuous ^6Be spectra. Two ^6Be detector systems were used in our measurements. Each system consisted of two rectangular parallel-plate silicon carrier detectors, 10 cm thick, 40 cm long, and 10 cm wide, mounted with 1 cm vertical separation.

A computer program was used to evaluate the ^6Be detector efficiency and to optimize the geometry. It was also used in extracting absolute cross sections. The geometry and efficiency calculations were experimentally checked by overlapping the angular range of the two ^6Be detectors. In order to match the ^6Be efficiencies of the two detectors, the distance to the target was 15 cm for the ^6Be detector placed at the forward angles and 17 cm for the one at backward angles. In this way the ^6Be effective solid angle varied by no more than a factor of 5 over the whole range of bombarding energies and measured angles (Fig.1). This corresponded to a mean angular aperture for ^6Be detection varying from two to three degrees in the c.m. system. The use of these rectangular sized detectors allowed for an efficiency improvement of a factor of about 10 with respect

For measuring the effuse and to get information on their location channels of 100 cm^2 ^{232}Th detector was mounted 100 cm from the target at 90° to the beam axis.

To measure the dead time each preamplifier test input was fed from a pulser triggered by the digital output from a beam current integrator. In the single and coincident spectra, this pulser peak was used to measure the effective beam charge taking into account dead time and pileup effects.

3. Data acquisition

In the ^{232}Th spectrum at incident α energies, the ^{212}Bi α peak from the ^{212}Bi decay into two ^{212}Po particles in their ground state can be obscured by other possible processes as for example when the ^{212}Bi particles are emitted in their first excited state or from the $^{212}\text{Bi} + \alpha$ decay of ^{212}Po . A two dimensional spectrum E_{212} versus E_{212} as shown in Fig.2, gives more information and allows better peak separation. The energy resolution ($\approx 4\%$) needs at least 128 channels for each dimension. This required too many channels to handle simultaneously coincidence and random spectra for two ^6Be detectors. However, based on the fact that the two dimensional spectrum is symmetrical with respect to the line $E_{212} = E_{212}$ (for identical gains) and that over the whole energy range of this study, the maximum energy difference between the two α -particles from a $^8\text{Be}(g.s.)$ decay is nearly constant ($\approx 2 \text{ MeV}$), the occupied memory size can be reduced by a coordinate change from E_{212}, E_{212} into $\Sigma = (E_{212} + E_{212})$,

to the target, $\theta = 0$ to 180° .

For most of the studies and to get information on their location, channels $100 < \theta < 180^\circ$ of the ^{12}C detector was mounted $100 < \theta < 180^\circ$ from the target at 90° to the beam axis.

To measure the dead time each preamplifier test input was fed from a pulser triggered by the digital output from a beam current integrator. In the energy and coincidence spectra, this pulser peak was used to measure the effective beam charge by taking into account dead time and pile-up effects.

3. Data Acquisition

In the α spectrum of ^{12}C incident energies, the ^{12}Be peak from the ^{12}C decay into two ^6Be particles in their ground state can be obscured by other possible processes as for example when the ^6Be particles are emitted in their first excited state or from the $^6\text{Be} + \alpha$ decay of $^{12}\text{C}^*$. A two dimensional spectrum $E_{\alpha 1}$ versus $E_{\alpha 2}$ as shown in Fig.2, gives more information and allows better peak separation. The energy resolution (ΔE) needs at least 128 channels for each dimension. This required too many channels to handle simultaneously coincidence and random spectra for two ^6Be detectors. However, based on the fact that the two dimensional spectrum is symmetrical with respect to the line $E_{\alpha 1} = E_{\alpha 2}$ (for identical gains) and that over the whole energy range of this study, the maximum energy difference between the two α -particles from a $^8\text{Be}(g.s.)$ decay is nearly constant (≈ 2 MeV), the occupied memory size can be reduced by a coordinate change from $E_{\alpha 1}, E_{\alpha 2}$ into $\Sigma = (E_{\alpha 1} + E_{\alpha 2})$,

$\sigma_{\text{total}} = \sigma_{\text{el}} + \sigma_{\text{in}} + \sigma_{\text{out}}$ and $\sigma_{\text{total}} = \sigma_{\text{el}} + \sigma_{\text{in}} + \sigma_{\text{out}}$ are the total, elastic, inelastic and nonelastic cross sections, respectively. The total cross section is the sum of the elastic and nonelastic cross sections. The inelastic cross section is the sum of the nonelastic and absorption cross sections. The absorption cross section is the sum of the capture and fission cross sections. The capture cross section is the sum of the radiative capture and nonradiative capture cross sections. The nonradiative capture cross section is the sum of the neutron capture and proton capture cross sections. The neutron capture cross section is the sum of the radiative neutron capture and nonradiative neutron capture cross sections. The proton capture cross section is the sum of the radiative proton capture and nonradiative proton capture cross sections.

REFERENCES

1. J. M. Blatt and V. F. Weisskopf, *Theoretical Nuclear Physics*, Wiley, New York, 1952.

2. R. G. Alston and J. M. Blatt, *Phys. Rev.* **100**, 100 (1955).

3. R. G. Alston and J. M. Blatt, *Phys. Rev.* **100**, 100 (1955).

4. R. G. Alston and J. M. Blatt, *Phys. Rev.* **100**, 100 (1955).

5. R. G. Alston and J. M. Blatt, *Phys. Rev.* **100**, 100 (1955).

6. R. G. Alston and J. M. Blatt, *Phys. Rev.* **100**, 100 (1955).

7. R. G. Alston and J. M. Blatt, *Phys. Rev.* **100**, 100 (1955).

8. R. G. Alston and J. M. Blatt, *Phys. Rev.* **100**, 100 (1955).

9. R. G. Alston and J. M. Blatt, *Phys. Rev.* **100**, 100 (1955).

10. R. G. Alston and J. M. Blatt, *Phys. Rev.* **100**, 100 (1955).

APPENDIX A

The excitation functions of $^{12}\text{C}(\alpha, n)^{13}\text{C}$ and $^{12}\text{C}(\alpha, p)^{13}\text{N}$ were measured simultaneously for the $^{12}\text{C}(\alpha, n)^{13}\text{C}$ and $^{12}\text{C}(\alpha, p)^{13}\text{N}$ reaction from $E_{\alpha} = 17$ to 33 MeV. Steps of 10-40 keV with thin targets were taken in some regions where narrow resonances could be expected, while 100 keV steps were used otherwise. The 48.0° angle, which corresponds to a zero of $P_6(\cos\theta)$, was chosen to identify any $J^{\pi} = 2^+$ level. A

states $J^{\pi} = 0^{+}$ and 2^{+} are represented in Fig. 3. The
 excitation function for the 0^{+} state was found to be dominant up
 to $E_{\alpha} = 10$ MeV. Below the measured excitation functions are shown
 in Fig. 3 the better known geometry and target thickness estimates
 taking into account carbon buildup, both absolute and relative cross
 sections differ slightly from our earlier work¹. Below $E_{\alpha} = 10$ MeV
 our data are in good agreement with those of
 Martin and Gehl⁵ and differ from those of Jones et al.⁶ by about
 20%. Our absolute cross sections are estimated to be accurate to
 within 20%.

Excitation functions corresponding to the elastic and
 inelastic channels from the α particles at 0^{+} are repre-
 sented in Fig. 4. They show no strong inter-channel correlation,
 except for a narrow resonance at $E_{\alpha} = 22.10$ MeV ($E_{X} = 21.06$ MeV)
 found previously by Hayward and Schmidt⁷ in elastic α scattering
 and which corresponds to a $J^{\pi} = 6^{+}$ level⁶. The decays of this
 level were measured simultaneously in the $^{12}\text{C} + \alpha$, $^{12}\text{C} + \alpha$,
 $^{12}\text{C} + \alpha$, $^6\text{Be}(g.s.) + ^6\text{Be}(g.s.)$ and $^{15}\text{N} + \alpha$ channels. All the
 resulting excitation functions show a resonant behavior (Fig. 5).
 It should be pointed out that this level has both a proton and a
 ^6Be width. Such a situation has already been observed for a $J^{\pi} = 4^{+}$
 state excited at $E_{\alpha} = 14.52$ MeV (Ref. 1). The analysis of the
 elastic scattering data (Fig. 5) using the phase shifts determined
 by Carter⁹, leads to the ratio $\Gamma_{\alpha} / \Gamma_{\text{Be}} = 0.06 \pm 0.02$ for the $J^{\pi} = 6^{+}$
 level. If we describe in a crude way the resonance at $E_{\alpha} = 22.10$ MeV
 in the $^{12}\text{C} + \alpha$ and $^6\text{Be}(g.s.) + ^6\text{Be}(g.s.)$ channels through Breit-

excitation functions for $J^{\pi} = 0^{+}$ state. Since the excitation functions for this level increase with E_{α} the contribution was found to be dominant up to $E_{\alpha} = 10$ MeV. Similarly, the measured excitation functions are shown in Fig. 5 for the better known geometry and target thickness estimate, taking into account carbon backscattering, both absolute and relative cross sections differ slightly from our earlier work⁶. Below $E_{\alpha} = 10$ MeV and at $\theta = 0^{\circ}$ the results are in good agreement with those of Martin and Gehl¹⁷ and differ from those of James et al.¹⁸ by about 20%. Our absolute cross sections are estimated to be accurate to within 20%.

Excitation functions corresponding to the elastic and inelastic channels from the π and π placed at 0° are represented in Fig. 4. They show no strong inter-channel correlation, except for a narrow resonance at $E_{\alpha} = 22.30$ MeV ($E_{\alpha} = 23.68$ MeV) found previously by Hayward and Schmidt⁷ in elastic α scattering and which corresponds to a $J^{\pi} = 0^{+}$ level⁶. The decays of this level were measured simultaneously in the $^{12}\text{C} + \alpha_2$, $^{12}\text{C} + \alpha_1$, $^{12}\text{C} + \alpha_2$, $^8\text{Be}(g.s.) + ^8\text{Be}(g.s.)$ and $^{15}\text{N} + \alpha$ channels. All the resulting excitation functions show a resonant behavior (Fig. 5). It should be pointed out that this level has both a proton and a ^8Be width. Such a situation has already been observed for a $J^{\pi} = 4^{+}$ state excited at $E_{\alpha} = 14.52$ MeV (Ref. 1). The analysis of the elastic scattering data (Fig. 5) using the phase shifts determined by Carter⁹, leads to the ratio $\Gamma_{\alpha_2} / \Gamma_{\alpha_1} = 0.06 \pm 0.02$ for the $J^{\pi} = 0^{+}$ level. If we describe in a crude way the resonance at $E_{\alpha} = 22.30$ MeV in the $^{12}\text{C} + \alpha_2$ and $^8\text{Be}(g.s.) + ^8\text{Be}(g.s.)$ channels through Breit-

excited state with $l = 0$ and $l = 1$ respectively. Taking into account the theoretical form of the angular distribution the results for the $^{10}\text{Be}(2,1)$ are given in Table 2.

TABLE 2. Angular distributions

Figure 7 shows the angular distribution of the $^{10}\text{Be}(2,1)$ in the energy range 1.0-1.5 MeV with experimental points and theoretical curves for $l = 0$ and $l = 1$ respectively. The angular distribution with $l = 0$ fits better over the experimental points.

Figure 8 shows results for the $^{10}\text{Be}(2,2)$ in the energy range 1.0-1.5 MeV. The angular distribution with $l = 2$ fits better than $l = 1$ and $l = 0$. The angular distribution with $l = 2$ fits better than $l = 1$ and $l = 0$ for increasing particle energies.

Despite the low efficiency for detecting $^{10}\text{Be}(2,1)$ and $^{10}\text{Be}(2,2)$ in their first excited states which was about 10% smaller than that for detecting $^{10}\text{Be}(2,0)$, it was still possible to measure some such angular distributions. In calculating the efficiency for the $^{10}\text{Be}(2,1)$ reaction, we assumed an isotropic correlation between the $^{10}\text{Be}(2,1)$ and the emitted α particle. In the energy range of the measurements (1.0-1.5 MeV), large cross sections are observed as can be seen in Fig. 7. Some angular distributions are strongly peaked near $\theta = 0^\circ$ and 180° for $^{10}\text{Be}(2,1)$ show a weak energy dependence.

of the $\sigma_{\text{tot}}^2(\theta)$ because of the general relation a general expression for the differential cross section is²

$$\frac{d^2\sigma}{d\Omega dE}(\theta, E) = \sum_{\text{even } l}^{L_{\text{MAX}}} |a_l(E)|^2 (2l+1) P_l(\cos \theta)^2 \quad (4.1)$$

where the $a_l(E)$ are complex numbers.

From (4.1) the total cross section is

$$\sigma(E) = \pi \sum_{\text{even } l}^{L_{\text{MAX}}} |a_l(E)|^2 \quad (4.2)$$

In this decomposition, each term represents the l -partial cross section.

The differential cross section can also be expressed linearly in terms of even Legendre polynomials. However, as the coefficients of this decomposition have no unique interpretation in terms of l -partial cross sections (except for the highest l value), formula (4.1) was used in a non-linear fitting program.

In Fig.8, we show the total and partial cross sections deduced from the angular distributions measured in this work (Fig.6), in the work of Chevallier et al.¹, and that of Martin and Ophel². Several sets of $|a_l(E)|^2$ values corresponding to about the same minimum σ^2 value were obtained for each angular distribution. The origin of this multiplicity arises from the fact that there is at least one ambiguity in the formula (4.1) for $L < L_{\text{MAX}}$ and also

VI. ANALYSIS

Let the L_{MAX} be given by the general relation a general expression for the differential cross section is²

$$\frac{d^2}{d\Omega dE} \sigma(E, \theta) = \sum_{\text{even } l}^{L_{\text{MAX}}} |a_l(E)|^2 |P_l(\cos \theta)|^2 \quad (4.1)$$

where the $a_l(E)$ are complex numbers.

From (4.1) the total cross section is

$$\sigma(E) = \pi \sum_{\text{even } l}^{L_{\text{MAX}}} |a_l(E)|^2 \quad (4.2)$$

In this decomposition, each term represents the l -partial cross section.

The differential cross section can also be expressed linearly in terms of even Legendre polynomials. However, as the coefficients of this decomposition have no unique interpretation in terms of l -partial cross sections (except for the highest l value), formula (4.1) was used in a non-linear fitting program.

In Fig.8, we show the total and partial cross sections deduced from the angular distributions measured in this work (Fig.6), in the work of Chevallier¹ and the work of Martin and Ophel². Several sets of $a_l(E)$ values corresponding to about the same minimum σ^2 value were obtained for each angular distribution. The origin of this multiplicity arises from the fact that there is at least one ambiguity in the formula (4.1) for L_{MAX} and also

measured with the help of a telescope camera. The angular region θ from 0° to 90° is divided into 10 equal parts. The data are recorded on a grid paper with a vertical bar of height 10 cm. The data are then plotted leaving the lowest of curves. The importance of the angular measurements can be seen particularly in the results of the work of Martin and myself¹ where angular distributions were given for the ^{137}Ba .

At least three different angular distributions of each measured angular distribution were obtained. The following is a brief interpretation of the data. In the present work, the angular distributions were decomposed into three parts while the others are unexplained. In general, the phases of these coefficients are found to be nearly constant when passing through the ^{137}Ba nucleus at different energies.

V. DISCUSSION

We consider first our data together with the data obtained in the incident energy range $E_\gamma = 1.15$ to 1.3 MeV. The angular decomposition of the cross sections, $\sigma(\theta) = \sigma_0 + \sigma_2 P_2(\cos\theta) + \sigma_4 P_4(\cos\theta) + \sigma_6 P_6(\cos\theta)$, is observed to be approximately $\sigma_0 = 0.15 \sigma_{\text{tot}}$, $\sigma_2 = 0.15 \sigma_{\text{tot}}$, $\sigma_4 = 0.15 \sigma_{\text{tot}}$, and $\sigma_6 = 0.55 \sigma_{\text{tot}}$. This suggested the existence of an ^{137}Ba rotational band with a very high moment of inertia, interpreted later as an 8 particle- 5 hole band⁵. One purpose of this study was to locate its $J^\pi = 8^+$ member.

A. Search for a $1^{\pi} = 8^{\pi}$ level

The excitation functions measured in the energy region $E_{\text{cm}} = 10 - 27$ MeV in 1 -MeV steps failed to show evidence for such a state. The same conclusion is reached after a search for an $1^{\pi} = 8^{\pi}$ level in the angular distributions. Up to $E_{\text{cm}} = 20$ MeV no evidence for such a term is found. About this energy, a weak but slowly increasing $1^{\pi} = 8^{\pi}$ component appears and becomes dominant at $E_{\text{cm}} = 23$ MeV (Fig. 8). Above $E_{\text{cm}} = 27$ MeV the non-linear fit indicates the presence of an $1^{\pi} = 10^{\pi}$ component. This implies that if a $1^{\pi} = 8^{\pi}$ level belonging to the predicted β particle-hole band exists below $E_{\text{cm}} = 20$ MeV, it would have a very different width from the other members of the band. One possibility to explain this difference in width is that the formation of this level might be inhibited either in the entrance or outgoing channels.

To test this hypothesis we report in Fig. 8 the energies corresponding to the grazing angular momentum given by the semiclassical formula

$$L(L+1) = k^2 R^2 (1 - 2\eta/kR) \quad (5.1)$$

where $R = R_0(A_1^{1/3} + A_2^{1/3})$, k and η are respectively the wave number and the Sommerfeld parameter for the considered channel. In the entrance channel ($R_0 = 1.4$ fm) the possibility of an inhibition for $1^{\pi} = 8^{\pi}$ is important below $E_{\text{cm}} = 20$ MeV. In the ${}^8\text{Be}(g.s.) + {}^8\text{Be}(g.s.)$ exit channel, the observed structures appear for each L value about 5 MeV below energies calculated with formula (5.1) and $R_0 = 1.4$ fm. However the agreement becomes quite satisfactory (Fig. 8) if we use

larger radius parameter $R_0 = 1.7$ fm. This might have been expected for the loose-molecule structure of the ${}^8\text{Be}$ nucleus¹³ and the ${}^8\text{Be}$ linear configuration molecule¹⁴ and the ${}^8\text{Be}$ nucleus. A particular inhibition can be expected in the outgoing channel.

B. Reaction mechanism

The broad structures observed in Fig. 8 are characterized by their appearance near the energies corresponding to the grazing angular momentum in the outgoing channel and by their energy localization for each L value. This behavior, where a single partial wave dominates within a restricted range of energy, is typical of a surface mechanism and can be explained by the formation of quasi-molecular states. This hypothesis is strengthened by the low cross sections for a direct mechanism estimated by extrapolation from higher incident energy results¹⁵ ($\sigma_{\text{el}} = 55$ MeV). These cross sections are about an order of magnitude lower than the observed ones.

A similar situation where resonance-like structures are observed near the Coulomb barrier is encountered in the study of reactions like ${}^{12}\text{C} + {}^{12}\text{C}$ or ${}^{12}\text{C} + {}^{10}\text{B}$ (Ref. 12). Most of the models developed to explain such behavior are based on two different hypotheses. The first assumes the formation of n -particle molecules^{13,14}. The conditions¹⁴ for the existence of these molecules are also fulfilled for the ${}^{12}\text{C}({}^8\text{Be}(g.s.)){}^8\text{Be}(g.s.)$ reaction. However the lack of apparent correlations with other exit channels like ${}^{12}\text{C} + \alpha_2$, ${}^{12}\text{C} + \alpha_1$ and ${}^{12}\text{C} + \alpha_1$ disfavors this hypothesis in our case. The second possibility is based on the creation of

V. SEARCH FOR A $J^{\pi} = 7^{-}$ LEVEL

The excitation functions measured in the energy region $E_{\text{lab}} = 10 - 27$ MeV in 1 MeV steps failed to show evidence for such a state. The same conclusion is reached after a search for an $l = 8$ term in the angular distributions. Up to $E_{\text{lab}} = 20$ MeV no evidence for such a term is found. About this energy, a weak but slowly increasing $l = 8$ component appears and becomes dominant at $E_{\text{lab}} = 21$ MeV (Fig. 8). Above $E_{\text{lab}} = 27$ MeV the non-linear fit indicates the presence of an $l = 10$ component. This implies that if a $J^{\pi} = 8^{-}$ level belonging to the predicted 8 particles hole band exists below $E_{\text{lab}} = 10$ MeV, it would have a very different width from the other members of the band. One possibility to explain this difference in width is that the formation of this level might be inhibited either in the entrance or outgoing channels.

To test this hypothesis we report in Fig. 8 the energies corresponding to the grazing angular momentum given by the semi-classical formula

$$L(L+1) = k^2 R^2 (1 - 2\eta/kR) \quad (5.1)$$

where $R = R_0(A_1^{1/3} + A_2^{1/3})$, k and η are respectively the wave number and the Sommerfeld parameter for the considered channel. In the entrance channel ($R_0 = 1.4 \text{ fm}$) the possibility of an inhibition for $l = 8$ is important below $E_{\text{lab}} = 20$ MeV. In the ${}^8\text{Be}(\text{g.s.}) + {}^8\text{Be}(\text{g.s.})$ exit channel, the observed structures appear for each L value about 5 MeV below energies calculated with formula (5.1) and $R_0 = 1.4 \text{ fm}$. However the agreement becomes quite satisfactory (Fig. 8) if we use

larger radius parameter $R = 1.7$ fm, which may have contributed to the observed loss of molecular structure in the $^{12}\text{C}(\text{g.s.}) + ^8\text{Be}(\text{g.s.})$ and the $^{12}\text{C}(\text{g.s.}) + ^8\text{Be}(\text{g.s.})$ linear configuration (reference 11) and the $^8\text{Be}(\text{g.s.})$ particular inhibition can be expected in the grazing channel.

B. Reaction mechanism

The broad structures observed in $\sigma_{\text{el}}(\theta, E)$ (Fig. 1) are characterized by their appearance near the energies corresponding to the grazing angular momentum for the grazing channel, and by their energy localization for each l value. This behavior, where a single partial wave dominates within a restricted range of energy, is typical of a *surface mechanism* and can be explained by the formation of quasimolecular states. This hypothesis is strengthened by the low cross sections for a direct mechanism estimated by extrapolation from higher incident energy results¹ ($E_{\text{lab}} = 75$ MeV). These cross sections are about an order of magnitude lower than the observed ones.

A similar situation where resonance-like structures are observed near the Coulomb barrier is encountered in the study of reactions like $^{12}\text{C} + ^{12}\text{C}$ or $^{12}\text{C} + ^{16}\text{O}$ (Ref. 12). Most of the models developed to explain such behavior are based on two different hypotheses. The first assumes the formation of α -particle molecules^{13,14}. The conditions¹⁴ for the existence of these molecules are also fulfilled for the $^{12}\text{C}(\text{g.s.}) + ^8\text{Be}(\text{g.s.})$ reaction. However the lack of apparent correlations with other exit channels like $^{12}\text{C} + \alpha_0$, $^{12}\text{C} + \alpha_1$ and $^{12}\text{C} + \alpha_2$ disfavours this hypothesis in our case. The second possibility is based on the creation of

quasimolecular states. Several tentative interpretations to reproduce the observed resonance-like structures have been done with optical model calculations using very shallow potentials¹⁵⁻¹⁸. We have made such an interpretation for the $^{12}\text{C}(\alpha, ^8\text{Be}(g.s.)) ^8\text{Be}(g.s.)$ reaction by using a statistical Hauser-Feshbach model calculation with the parameters given in Table II. This calculation is not well adapted to all the incident energies of this study due to the small level densities and number of open channels in the ^{15}O nucleus for lower excitation energies. The heavy ion optical potential used to describe the $^8\text{Be} + ^8\text{Be}$ scattering must have a very small imaginary part in order to reproduce the observed structures which are only produced by the transmission coefficients relevant to the outgoing channel. In Fig. 5 the calculated curves (dashed lines) are compared to the experimental data. The similitude between the broad predicted structures and the behavior of the experimental cross sections is in surprising agreement with the nuclear molecule hypothesis. Recent results obtained for the $^{10}\text{B}(\alpha, ^8\text{Be}) ^{12}\text{C}$ reaction²² show a different behavior which could imply that the structures are due to the simultaneous presence of two ^8Be nuclei.

VI. CONCLUSION

In the energy range $E_{\alpha} = 17 - 33$ MeV of this study only one narrow resonance, corresponding to a $J^{\pi} = 6^{+}$ level, is found at $E_{\alpha} = 22.30$ MeV. Below $E_{\alpha} = 20$ MeV, the existence of a $J^{\pi} = 8^{+}$ level cannot be definitively ruled out, as it may be possible that the limited amount of angular momentum in the entrance channel inhibits

quasimolecular states. Several tentative interpretations to reproduce the observed resonance-like structures have been done with optical model calculations using very shallow potentials¹⁵⁻¹⁸. We have made such an interpretation for the $^{12}\text{O}(\alpha, ^8\text{Be})\text{s.}(\alpha)^8\text{Be}(\text{g.s.})$ reaction by using a statistical Hauser-Feshbach model calculation with the parameters given in Table II. This calculation is not well adapted to all the incident energies of this study due to the small level densities and number of open channels in the ^{16}O nucleus for lower excitation energies. The heavy ion optical potential used to describe the $^6\text{Be} + ^6\text{Be}$ scattering must have a very small imaginary part in order to reproduce the observed structures which are only produced by the transmission coefficients relevant to the outgoing channel. In Fig. 8 the calculated curves (dashed lines) are compared to the experimental data. The similitude between the broad predicted structures and the behavior of the experimental cross sections is in surprising agreement with the nuclear molecule hypothesis. Recent results obtained for the $^{16}\text{O}(\alpha, ^8\text{Be})^{12}\text{C}$ reaction²² show a different behavior which could imply that the structures are due to the simultaneous presence of two ^8Be nuclei.

VI. CONCLUSION

In the energy range $E_1 = 17 - 33$ MeV of this study only one narrow resonance, corresponding to a $J^\pi = 6^+$ level, is found at $E_2 = 22.30$ MeV. Below $E_3 = 20$ MeV, the existence of a $J^\pi = 8^+$ level cannot be definitively ruled out, as it may be possible that the limited amount of angular momentum in the entrance channel inhibits

the formation of a complex.

The analysis of the measured angular distribution allows the extraction of differential cross sections. The broad resonant structure observed near the Coulomb barrier in the fitting channel is characterized by the successive appearance of $l = 0, 1, 2, \dots$ partial waves and the energy localization of these structures at each l value. It is related to the exit channel and may be attributed to the formation of nuclear molecules, whenever the different behavior recently²² will make it interesting to study their l -dependence when some l values are $l = 0$.

As a result of the present work, the authors are very grateful to the staff of the

Table 1. Parameters of the $1^{-} + 6^{+}$ level at $E_X = 21.68$ MeV in ^{10}B

| E_T MeV ^a | Q (keV) | Q_{Be} (keV) | Q_1 (keV) | Q_2 (keV) |
|-------------------------------|-----------------------|--------------------------|----------------|----------------|
| 21.295 ± 0.015 | 25 ± 5 | 3.5 | 15 ± 0.5 | ≈ 6 |
| $21.306 \pm 0.006^{\text{a}}$ | $26 \pm 4^{\text{a}}$ | | | |

^a Ref. 6

Table 1. Parameters of the $\pi^+ + \pi^+$ level at $E_{\pi} = 23.68$ MeV in ^{16}O

| E_{π} MeV | Γ (keV) | Γ_{Be} (keV) | Γ_{Be} (keV) | Γ_{Be} (keV) |
|-------------------------------|-----------------------|-------------------------------|-------------------------------|-------------------------------|
| 22.295 ± 0.015 | 25 ± 5 | 3.5 | 1.5 ± 0.5 | ≈ 6 |
| $22.304 \pm 0.005^{\text{a}}$ | $26 \pm 4^{\text{a}}$ | | | |

^a Ref. 6

Table II. Optical model parameters used in the present calculation. The level density equations and the reaction parameters are those defined by Gilbert and Cameron.¹⁴ The form of the potentials are defined in Ref. 15.

| Channel | E MeV | R_0^A (fm) | V_0 fm | W_0^B (MeV) | R_0^A (fm) | V_0 (MeV) | R_0^A fm | W_0^A fm | R_0^A fm | Ref. |
|----------------------------|-------------------|-----------------|-------------|------------------|-----------------|----------------|---------------|---------------|---------------|------|
| $^{10}\text{Be}_p$ | 90.5 ^a | 1.25 | 0.65 | 11.5 | 1.25 | 0.47 | 5.5 | 1.26 | 1.25 | 16 |
| $^{12}\text{C}_n$ | 98 | 1.25 | 0.65 | 8.5 | 1.25 | 0.48 | 5.5 | 1.25 | 1.25 | 16 |
| $^{14}\text{N}_d$ | 65 | 1.15 | 0.60 | 12 | 1.16 | 0.48 | | | | 16 |
| $^{16}\text{O}^3\text{He}$ | 158 | 1.61 | 0.60 | 6.8 | 2.15 | 0.65 | 6 | 1.65 | 1.6 | 16 |
| $^{16}\text{O}_d$ | 150 | 1.26 | 0.65 | 23 | 1.65 | 0.58 | | | | 16 |
| $^{16}\text{O}_n$ | 185 | 1.4 | 0.52 | 25 | 1.4 | 0.54 | | | | 16 |
| $^8\text{Be}^8\text{Be}$ | 10.8 ^e | 1.4 | 0.45 | 5.5 | 1.4 | 0.45 | | | | 16 |

^a $R = R_0 A_2^{1/3}$ except in the $^{10}\text{Be} + ^8\text{Be}$ channel where $R = R_0 (A_1 + A_2)$. (A_1 and A_2 are respectively the mass number of the light and heavy particles in the considered channels). The Coulomb radius is equal to the radius of the real well.

^b The imaginary well is of the surface type for the $^{12}\text{C}_n$ and $^{14}\text{N}_d$ channels, of the Gaussian type in the $^{16}\text{O}_n$ channel and all others are of the volume type.

^c Ref. 20.

^d Ref. 23.

^e The $^8\text{Be} + ^8\text{Be}$ optical potential is adapted from the one used by Maher et al.²¹

^f Energy above which continuum level densities are used.

1. The development of the β function for the renormalized coupling constant in the ϕ^4 theory, *Phys. Rev. D*, 12, 1512 (1975).
2. G. Martin and J. Lucy, *Phys. Rev. D*, 12, 1517 (1975).
3. J. S. James, Ed., *Alpha-Magnetic Resonance*, in *Nuclear Magnetic Resonance*, Proceedings of the 1974 International Conference on Nuclear Magnetic Resonance, Max Planck Institute for Physics and Astrophysics, Munich, Germany, 1974, Springer-Verlag, New York, 1975, p. 107.
4. E. M. Lifshitz, *Physical Kinetics*, in *Physical Kinetics*, 2nd Edition, Butterworths, London, 1969, p. 107.
5. J. S. James, *Phys. Rev. D*, 12, 1520 (1975).
6. J. S. James, *Phys. Rev. D*, 12, 1521 (1975).
7. J. S. James, *Phys. Rev. D*, 12, 1522 (1975).
8. J. S. James, *Phys. Rev. D*, 12, 1523 (1975).
9. J. S. James, *Phys. Rev. D*, 12, 1524 (1975).
10. V. Anselmi, K. Fujikura, and M. Taroni, *Ann. Phys.*, 81, 1 (1973).
11. Nuclear Energy, edited by M. Taroni, Academic Press, New York, 1974, p. 107.
12. G. W. Leibniz, *N.A.S. Trans.*, and *Philos. Trans.*, 170, 171 (1702).
13. H. Stiemssen, in *Nuclear Spectroscopy and Radioisotopes*, 1974, Academic Press, New York, 1974, p. 107.
14. G. L. Montroll and R. W. Vogt, *Phys. Rev.*, 122, 107 (1961).
15. H. Vort, P. Dieck, W. Gaister, F. Hahnle, G. Hartmann, G. H. Heide, F. Siller, and G. Isenens, *Z. Phys.*, 222, 107 (1969).

- ¹ S.M. Yegorov and L. S. Neftin, Phys. Lett. 418, 3 (1972).
- ² S. Imanishi, Nucl. Phys. A 124, 33 (1969).
- ³ J. Vogt and H. McManus, Phys. Rev. Lett. 4, 518 (1960).
- ⁴ K.W. McVoy, Phys. Rev. 131, 1104 (1971).
- ⁵ A. Gilbert and A.J.W. Cameron, Can. J. Phys. 33, 1246 (1965).
- ⁶ N. Austern, Direct Nuclear Reaction Theories, Edited by R.E. Marshak (John Wiley and Sons, New York, 1970), p. 109.
- ⁷ J.V. Maher, M.W. Sachs, P.H. Siemssen, A. Weidinger, and D.A. Bromley, Phys. Rev. 155, 1665 (1969).
- ⁸ J. Rudolf, Nucl. Phys. A 115, 177 (1968).
- ⁹ J. Rudolf, Nucl. Phys. A 124, 532 (1969).

8. N. Nigmatulin and T. S. Neutchen, *Phys. Lett.*, 218, 14 (1972).
- ⁹ S. Imanishi, *Nucl. Phys.*, A124, 33 (1969).
- ¹⁰ J. Vogt and H. McManis, *Phys. Rev. Lett.*, 4, 318 (1960).
- ¹¹ R.W. McVoy, *Phys. Rev.*, 11, 1104 (1971).
- ¹² A. Gilbert and A.G.W. Cameron, *Can. J. Phys.*, 33, 1446 (1965).
- ¹³ N. Austern, *Direct Nuclear Reaction Theories*, Edited by R.E. Marston (John Wiley and Sons, New York, 1973), p. 109.
- ¹⁴ J.V. Maher, M.W. Sachs, P.H. Stenssen, A. Weidinger, and D.A. Bromley, *Phys. Rev.*, 156, 1065 (1969).
- ¹⁵ J. Rudolf, *Phys. Rev. Lett.*, 21, 1115 (1968).
- ¹⁶ J.A. Tjon and J.M. Eisenberg, *Nucl. Phys.*, A124, 512 (1969).

(see Sec.III A). The dashed lines are to guide the eye.

Fig. 6 Angular distributions in the c.m. observed at several bombarding energies for the $^{12}\text{C}(\alpha, {}^8\text{Be}(g.s.)) {}^8\text{Be}(g.s.)$ reaction. The solid lines are the results of a non-linear fit to the data with the formula (4.1) (see Sec.IV). Here E_B stands for the bombarding energy.

Fig. 7 Angular distributions in the c.m. measured at several bombarding energies for the $^{12}\text{C}(\alpha, {}^8\text{Be}(2.9 \text{ MeV})) {}^8\text{Be}(g.s.)$ reaction.

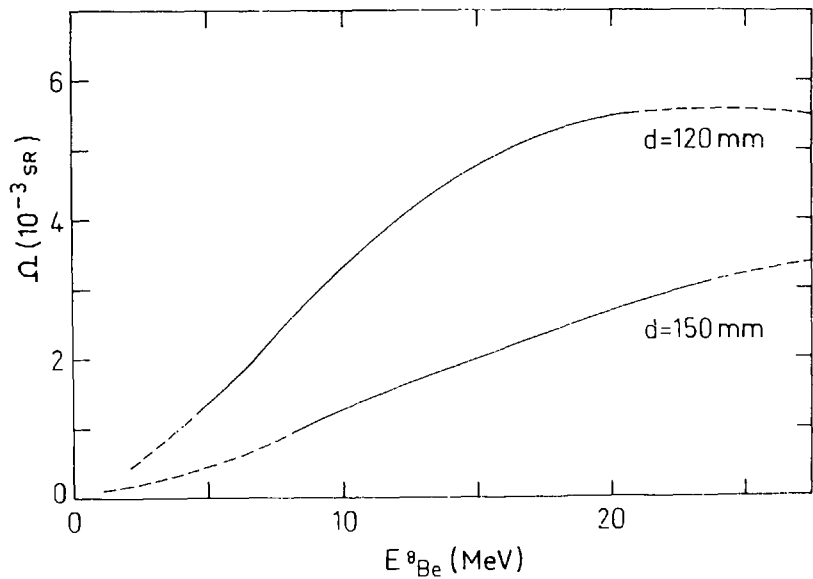
Fig. 8 Total and l-partial cross sections of the $^{12}\text{C}(\alpha, {}^8\text{Be}(g.s.)) {}^8\text{Be}(g.s.)$ reaction for $E_\alpha = 12 - 34 \text{ MeV}$. The solid lines are to guide the eye and correspond to the general trend of the measured differential cross sections. The dashed lines correspond to the results of a statistical Hauser-Feshbach compound nuclear calculation done with the parameters given in Table II. The solid and open triangles represent respectively the energies corresponding to the grazing angular momentum (see Sec.V(A)) for the entrance and outgoing channels. The arrows show the position of the $J^\pi = 2^- - 6^+$ levels of the 8 particle-hole band² and the predicted position of the $J^\pi = 8^+$ member of this band assuming a $2j+1$ rule. The solid bars correspond to the decomposition of the angular distributions measured in this work in l partial waves (see Sec.V). The dashed bars correspond to the decomposition of the measurements of Martin and Spinel².

see Sec.III A). The dashed lines are to guide the eye.

Fig. 6 Angular distributions in the c.m. observed at several bombarding energies for the $^{12}\text{C}(\alpha, {}^6\text{Be}(g.s.)) {}^8\text{Be}(g.s.)$ reaction. The solid lines are the results of a non-linear fit to the data with the formula (4.7) (see Sec.IV). Here E_B stands for the bombarding energy.

Fig. 7 Angular distributions in the c.m. measured at several bombarding energies for the $^{12}\text{C}(\alpha, {}^7\text{Be}(2.9\text{ MeV})) {}^8\text{Be}(g.s.)$ reaction.

Fig. 8 Total and l-partial cross sections of the $^{12}\text{C}(\alpha, {}^6\text{Be}(g.s.)) {}^8\text{Be}(g.s.)$ reaction for $E_{\alpha} = 12 - 34\text{ MeV}$. The solid lines are to guide the eye and correspond to the general trend of the measured differential cross sections. The dashed lines correspond to the results of a statistical Hauser-Feshbach compound nuclear calculation done with the parameters given in Table II. The solid and open triangles represent respectively the energies corresponding to the grazing angular momentum (see Sec.V(A)) for the entrance and outgoing channels. The arrows show the position of the $J^{\pi} = 2^{\pi} - 6^{\pi}$ levels of the 8 particle-hole band² and the predicted position of the $J^{\pi} = 8^{\pi}$ member of this band assuming a $2J - 1$ rule. The solid bars correspond to the decomposition of the angular distributions measured in this work (see Introduction). The dashed bars correspond to the decomposition of the measurements of Martin and Lynn¹⁷.



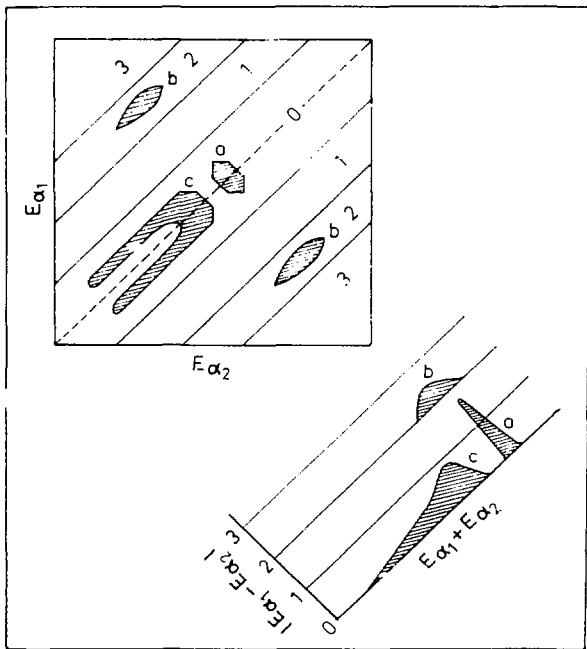


Fig. 2.

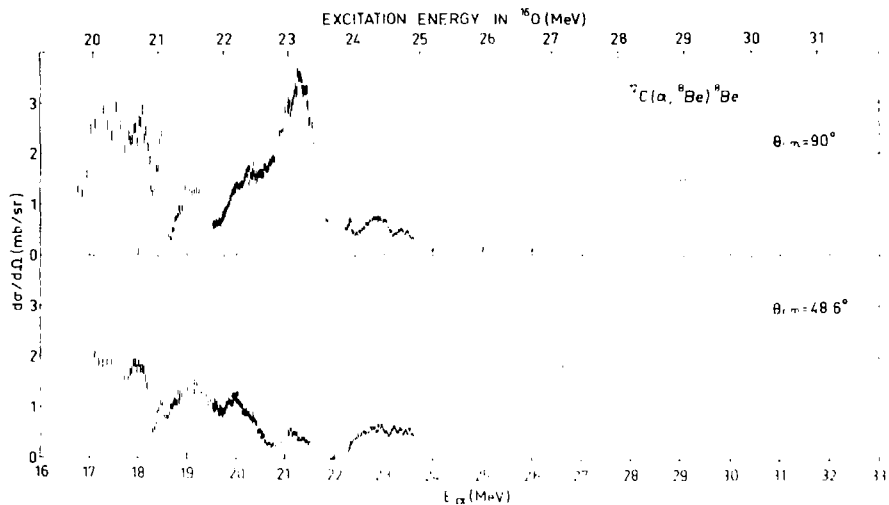


FIG. 2.

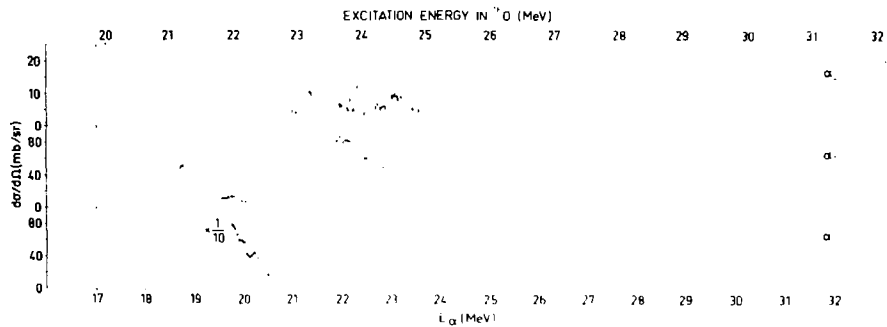
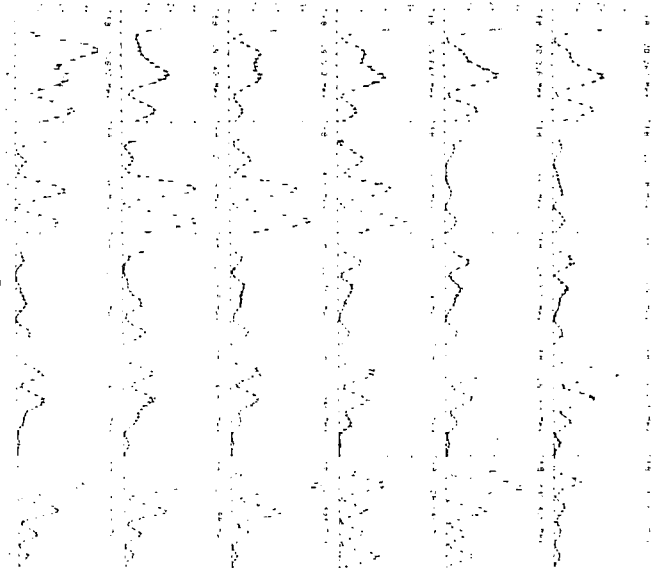
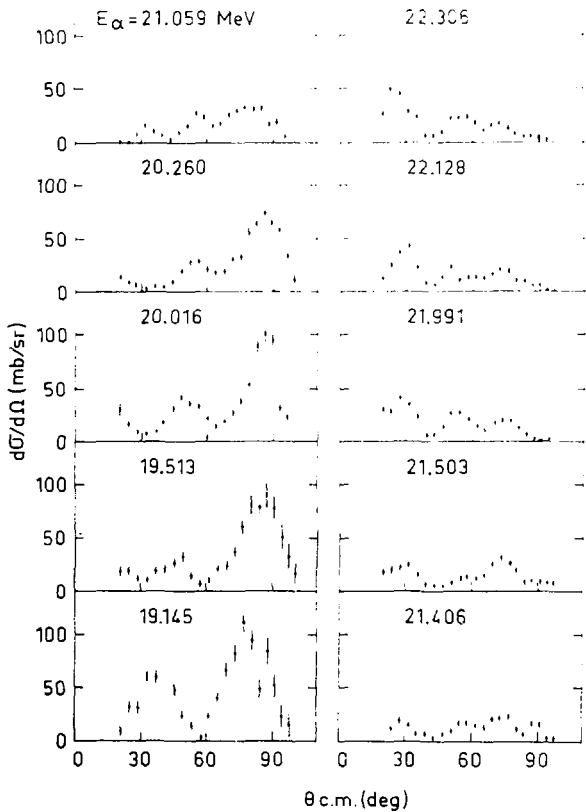


Fig. 11

$\theta_{cm}(\text{deg})$

$d\sigma/d\Omega$ (mb/sr)





10 Mev

35

TOTAL CROSS SECTION FOR
THE $^{10}\text{B}(n,\alpha)^7\text{Li}$ REACTION

